Evolution of the Muon Distribution in the g-2 Ring

David L. Rubin

July 18, 2016

1 Introduction

Muons injected into the g-2 storage ring execute betatron oscillations about a closed orbit. The closed orbit is defined by the magnetic and electric fields and the muon energy. If the magnetic field is uniform and the quadrupole electric field linear in the displacement of the muons from the closed orbit, then all muons oscillate with the same betatron frequencies, independent of amplitude. However, in the g-2 ring, the fields of the electrostatic quadrupoles have significant nonlinearity. The result is that the betatron frequency depends on the amplitude of the oscillations. A distribution that is initially executing coherent centroid motion, or coherent modulation of its width, will eventually decohere on a time scale that depends on the nonlinearity and the emittance (distribution of amplitudes). We will show how the decoherence time is related to oscillation amplitude and quad multipoles.

In addition, the closed orbit, the betatron tunes, and the revolution frequency are all energy dependent. As a result of this energy dependence, muons in a distribution with finite energy spread will execute betatron oscillations about their respective closed orbits with a spread of frequencies. Again the frequency spread evolves a decoherence of the betatron motion. The amplitude of the motion of the centroid of the distribution, as well as the modulation of the beam width, will "damp" over this decoherence time. We will show how the chromaticity (energy dependence of betatron tunes) is related to the focusing index in the g-2 ring.

Conversely, we find that because of the momentum dependence of the cyclotron period, and the dispersion mismatch at the inflector exit, coherent centroid motion can emerge from an initially incoherent distribution. The "fast rotation" analysis takes advantages of the correlation of cyclotron frequency and momentum to measure the distribution of momenta. The "fast rotation" signal is a measure of the time dependence of the intensity of the distribution, where intensity is proportional to the number of muons per unit time. The coherent betatron oscillation is a measure of the time dependence of the position of the centroid of the distribution. We will develop analytic expressions for both.

Evidently, particles that oscillate coherently at the start of the fill, will decohere due to both amplitude and energy dependence of the betatron tunes. The amplitude of the modulation of the width of the injected beam, results from the mismatch of the twiss parameters at the inflector exit. The intial amplitude of the oscillations of the beam centroid will depend on the quality of the fast kicker pulse. As the betatron frequency depends on the amplitude and energy of the particles, the modulation of the width, as well as the oscillations of the centroid, will decohere after some number of turns. We also find that the dispersion mismatch leads to a coherent betatron oscillation that persists for more than 1000 turns.

2 Amplitude Dependent Tune

In this section the we show how amplitude dependence of the tune is related to the quadrupole multipoles. The multipole expansion of the quadrupole field in the midplane of the ring can be

written[1]

$$E_x(x) = \sum_{n=1} b_n n \frac{x^{n-1}}{r_0^n}$$

The effective focusing of the quadrupoles is proportional to the field gradient

$$G_x = \frac{\partial E_x}{\partial x} = \sum_{n=1} n(n-1) b_n \frac{x^{n-2}}{r_0^n}$$

In a perfect quadrupole, only b_2 is non-zero and $G_x = 2b_n \frac{1}{r_0^2}$, independent of displacement x. In our imperfect quadrupole, the gradient depends on the amplitude. We write an effective amplitude dependent gradient

$$\langle G_x \rangle = \sum_{n=1} n(n-1) b_n \frac{\langle x^{n-2} \rangle}{r_0^n}$$

where $\langle x^{n-2} \rangle$ is the average of x^{n-2}. Let's assume that $x = x_0 \cos(\omega_{cbo} t)$, a reasonable assumption in our ring where $\beta(s)$ is very nearly constant. Then

$$\langle G_x \rangle = \sum_{n=1} n(n-1) b_n \frac{x_0^{n-2}}{r_0^n} \langle \cos^{n-2}(\omega t) \rangle \tag{1}$$

$$\tag{2}$$

and the contribution from all odd n is zero. The effective gradient is then given by

$$G_A(x_0) = \sum_{n=1}^{N} n(n-1) b_n \frac{x_0^{n-2}}{r_0^n} c_{n-2}$$

where $c_{n-2} = \langle \cos^{n-2} \omega t \rangle$ and x_0 is the amplitude. The multipoles for the g-2 ring quadrupoles are summarized in Table 1.

The tune shift due to an electric field gradient error $G(s)$ is

$$\Delta Q = \frac{1}{4\pi} \oint \beta q \frac{E_x(s)}{dx} \frac{1}{pv} ds$$

Table 1:

Multipole (n)	Value [V/m^n]	c_{n-2}	$\Delta Q_x/m^n$
2	26331.0	0	0
4	43.06	1/2	1.26×10^8
6	-59.90	3/8	-1.08×10^{11}
8	-7.18	5/16	-8.96×10^{12}
10	-510.63	35/128	-4.22×10^{17}
12	-8.48	63/256	-4.44×10^{18}
14	68.25	231/1024	2.19×10^{22}

where q, p, and v are the muon charge, momentum and velocity respectively. Using $R = \gamma mv/qB$ the tune shift becomes

$$\Delta Q = \frac{1}{4\pi} \oint \beta \frac{E_x(s)}{dx} \frac{1}{RBv} ds$$

Then the amplitude dependent tune shift is

$$\Delta Q(x,s) = \frac{1}{4\pi} \oint \beta \frac{G_A(x,s)}{RBv} ds$$

The gradient $G_A(s)$ is given by Equation 1 in the quads and is zero everywhere else. Since the quads extend over a length $L = 4(2\pi\frac{39}{360}(7.112))$ we write

$$\Delta Q(x,s) = \frac{1}{4\pi} \beta \frac{G_A(x,s)}{RBv} L \tag{3}$$

The contribution to the horizontal tune shift from each of the multipoles is shown in Table 1 and in Figure 1.

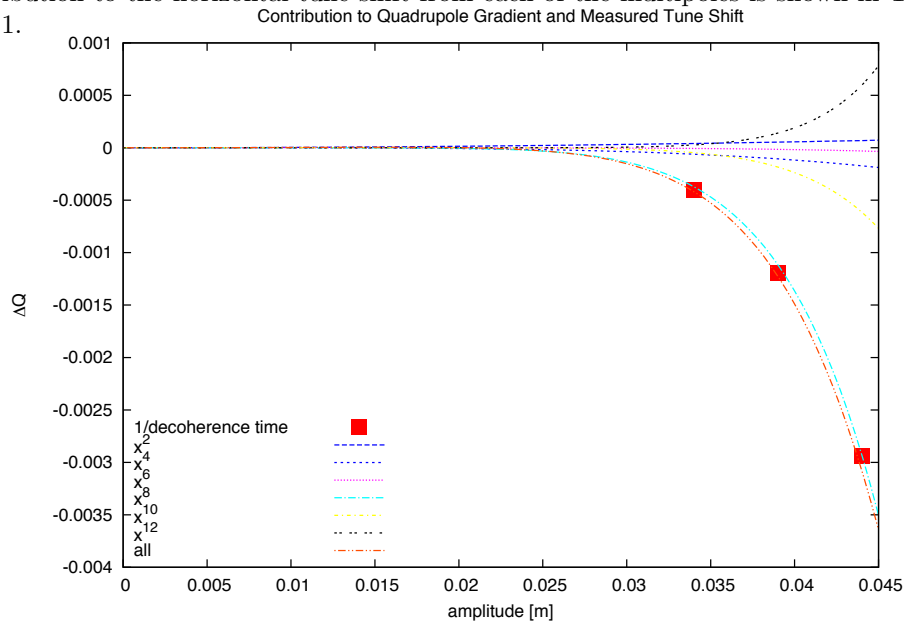

Figure 1: Tuneshift as a function of betatron amplitude (Equation 3 for each of the quadrupole multipoles (lines) and as computed in tracking simulation (squares) for three different amplitudes.

3 Tune spread and decoherence

The analytic calculation of the amplitude dependent tune shifts can be checked in simulation. The simulation is built from routines in the BMAD accelerator library. The fields of the electrostatic-quadrupoles are represented in terms ofthe multipoles expansion described above.

Suppose the tunes for two different muons are split by ΔQ. The sum of the displacements of the two muons at Q and $Q + \Delta Q$ on turn n is

$$x(n) \quad = \quad A\sin(2\pi Q n) + A\sin(2\pi(Q + \Delta Q)n)$$

where $\bar{Q}$ is the average of the tunes. Note that if $n\Delta Q = \frac{1}{2}$ then the particles are 180° out of phase. The decoherence time (in units of turns) is $T = \frac{1}{2\Delta Q}$. Track two particles with initial amplitudes of about 4 cm. For one of the particles, turn off all multipoles $n > 2$ so that the guide field is linear and tune is independent of amplitude. For the other, restore all quad multipoles. The oscillation of the two particles is shown superimposed in Figure 2.

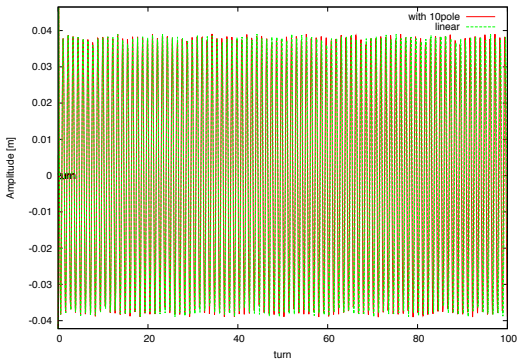

Figure 2: Horizontal displacement vs turn number. The green line is with purely linear quadrupole fields, (no multipoles). The red line is with all quad multipoles included. The amplitude of the oscillation is about 3.9 cm.

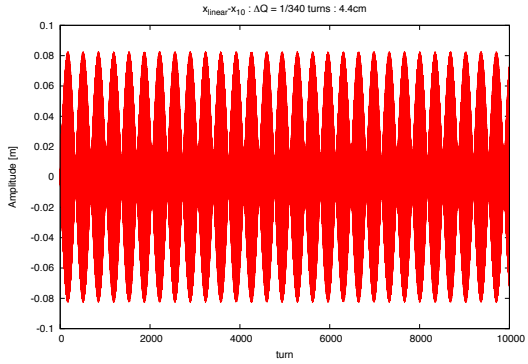

Figure 3: Sum of displacements with and without quad multipoles when the oscillation amplitude is 4.4 cm. The beat frequency corresponds to the tune difference.

The sum of the displacements of the two particles is

$$\begin{aligned} x_1(n) + x_2(n) &= A\left(\sin(2\pi(\bar{Q} + \Delta Q/2)n) + \sin(2\pi(\bar{Q} - \Delta Q/2)n)\right) \\ &= A\left(\sin(2\pi(\bar{Q} + \Delta Q/2)n) + \sin(2\pi(\bar{Q} - \Delta Q/2)n)\right) \\ &= 2A\sin(2\pi\bar{Q}n)\cos(2\pi\Delta Q n) \end{aligned}$$

and shown in Figure 3. The signal at $\bar{Q}$ is modulated at the tune difference. From Figure 3, we see that $\Delta Q(44\text{mm})$ is 1/340 turns.

We use the same strategy to determine the tune shift for amplitudes of 39 mm and 34 mm. The turn by turn sum of trajectories with and without quad nonlinearities are shown in Figures 4 and 5 respectively. The amplitude dependence of the tune shift as determined by tracking is plotted in Figure 1 along with the analytic calculation. Analytic and numerical results are in reasonable agreement.

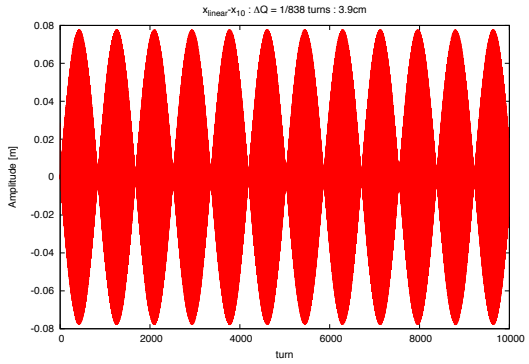

Figure 4: Sum of displacements with and without quad multipoles (nonlinearities) when the oscillation amplitude is 3.9 cm as in Figure 2. $\Delta Q = 1/838$ turns.

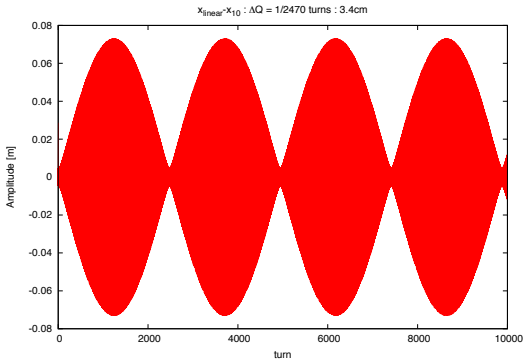

Figure 5: Sum of displacements with and without quad multipoles when the oscillation amplitude is 3.4 cm. $\Delta Q = 1/2470$ turns.

4 Decoherence in a distribution

Consider a distribution of 1000 muons with 95% horizontal and vertical emittance of 40mm-mrad. Suppose the residual coherent betatron oscillation amplitudes are 10mm horizontally and about 1mm vertically. Due to the beta mismatch the width of the distribution varies from 6 to 13 mm and the height from 8 to 16mm. As described above, the effect of the quadrupole nonlinearity is to introduce an amplitude dependent tuneshift. Vertical and horizontal centroid and width over the first 2000 turns are shown in Figure 6. Here the quad nonlinearity is turned off so there is no decoherence. The decoherence is evident in the evolution of the distribution with quad nonlinearity restored as shown in Figure 7. The amplitude of the coherent horizontal betatron oscillation shrinks by a factor of two in 2000 turns. The variation in the width and height of the distribution also "damps" on a time scale of 1000 turns. Note that the particles remain bunched, as they all have the same energy.

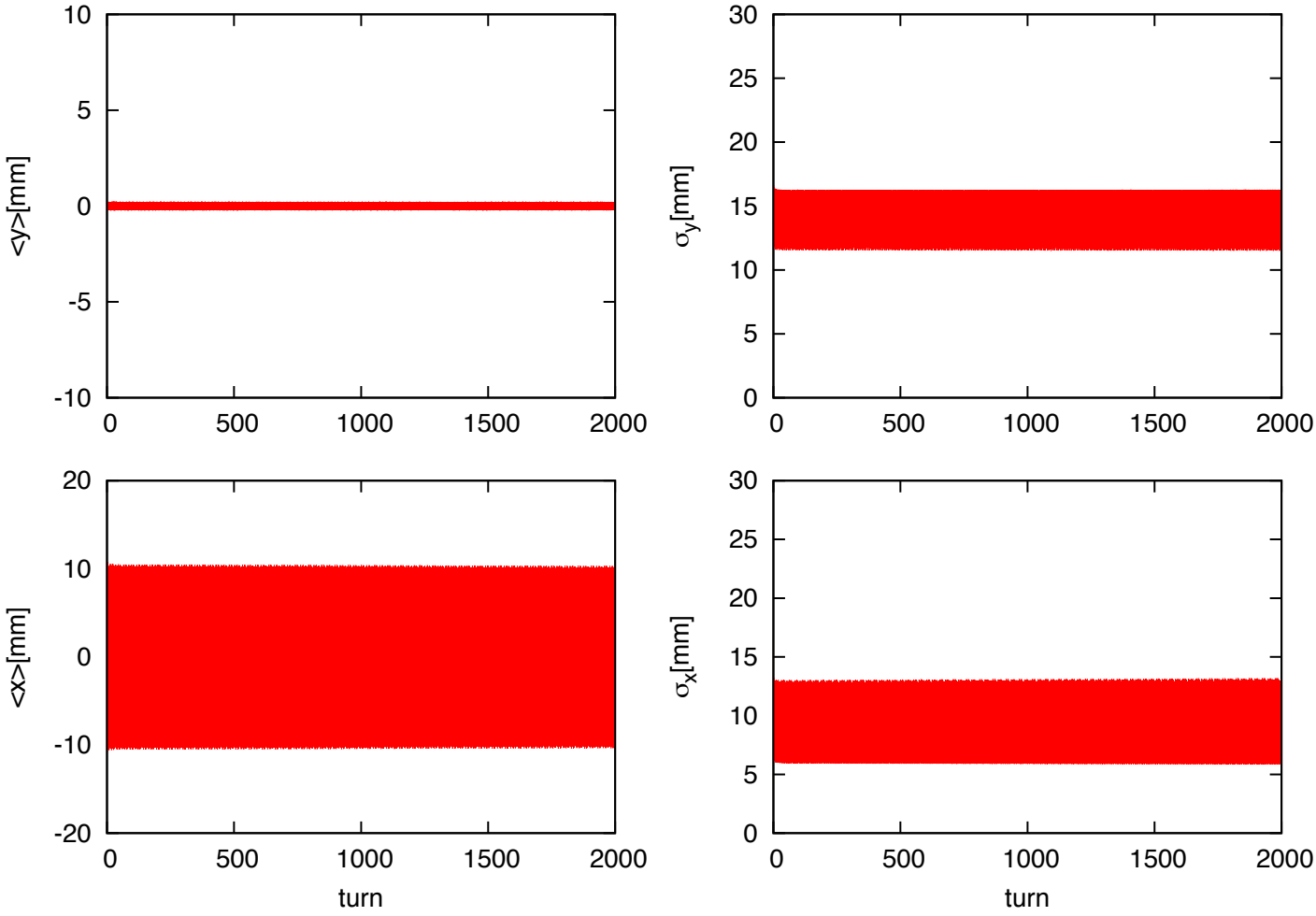

Figure 6: With no quad nonlinearities, average horizontal (bottom-left) and vertical (top-left) centroid motion versus turn. Horizontal and vertical beam width versus turn is at right.

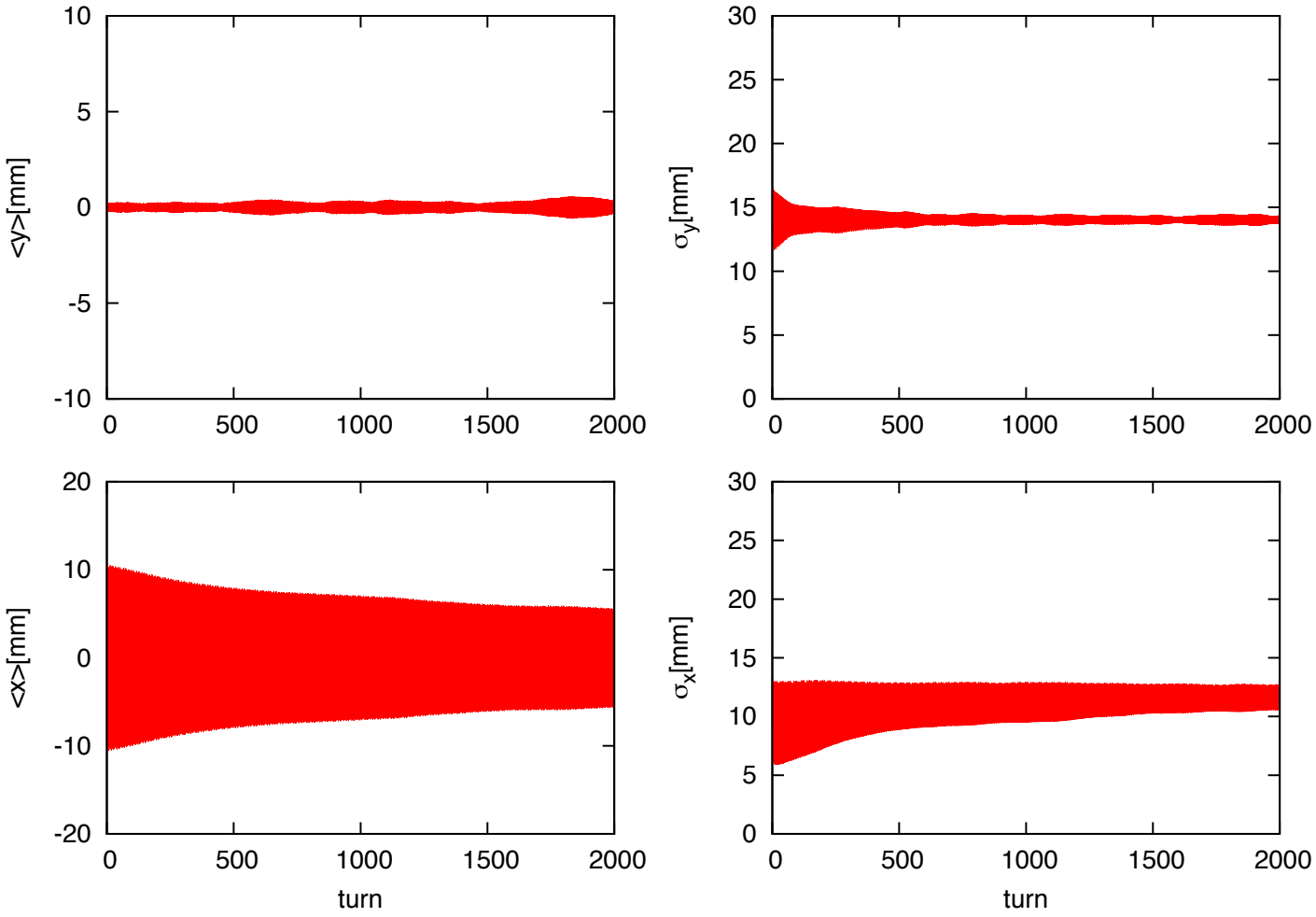

Figure 7: With quad linearities, average horizontal (bottom-left) and vertical (top-left) centroid motion versus turn. Horizontal and vertical beam width versus turn is at right. Decoherence of centroid motion and modulation of beam width is evident.

5 Momentum spread

The energy dependence of the betatron tunes and the revolution frequency, contribute to the evolution and decoherence of betatron motion due to the finite energy spread in the beam. In a cyclotron with electrostatic focusing distributed uniformly around the ring, the tune depends on the focusing index n according to

$$\begin{aligned} Q_x &= \sqrt{1-n} \\ Q_y &= \sqrt{n} \end{aligned}$$

where

$$n = \left(\frac{r}{v_s B}\right)\frac{\partial E_r}{\partial r}$$

r is the radius of curvature of the on momentum muon in magnetic field B and v_s is the azimuthal velocity, that is $r = \frac{\gamma m v_s}{qB} = \frac{p}{qB}$. The dependence of betatron tune on energy, (chromaticity) follows from

$$n(\delta) = \frac{p(1+\delta)}{q v_s B^2}\frac{\partial E_r}{\partial r}$$

so that

$$\begin{aligned} \frac{\partial Q_x}{\partial \delta} &= -\frac{1}{2}\frac{1}{\sqrt{1-n}}\frac{\partial n}{\partial p} = -\frac{n}{2\sqrt{1-n}} = \frac{Q_y^2}{2Q_x} = -0.103 \\ \frac{\partial Q_y}{\partial \delta} &= \frac{n}{2\sqrt{n}} = \frac{1}{2}Q_y = 0.215 \end{aligned}$$

evaluated for $n = 0.185$. An important assumption in the above is that the electrostatic quadrupoles extend continuously around the circumference of the ring which is not the case in the g-2 ring. To understand the implications for chromaticity it is useful to distiguish three contributions; energy dependence of quadrupole focal length, energy dependence of pathlength and effect of quad curvature.

The horizontal and vertical tunes are written in terms β-function

$$Q_{h/v} = \frac{1}{2\pi}\oint \frac{1}{\beta_{h/v}} ds \tag{4}$$

In a ring with constant β ($\frac{d\beta}{ds} = 0$), we have that $K = 1/\beta^2$ and the tunes are

$$\begin{aligned} Q_{h/v} &= \frac{1}{2\pi}\oint \sqrt{K_{x/y}} ds \\ Q_{h/v} &= \sqrt{K_{x/y}} R \end{aligned} \tag{5}$$

where

$$\begin{aligned} K_x &= \frac{1}{\rho^2} - \frac{q}{mv^2}\frac{\partial E}{\partial r} = \frac{1}{\rho^2} - J \\ K_y &= \frac{q}{mv^2}\frac{\partial E}{\partial y} \end{aligned}$$

where for convenience we define $J \equiv \frac{q}{mv^2}\frac{\partial E}{\partial r} = n$ and note that $Q_y = \sqrt{J}$.

The three distinct contributions to the chromaticity are enumerated.

1. The effective gradient (K) decreases with energy, increasing horizontal and decreasing the vertical tune.

$$\begin{aligned}\frac{\partial K_x^{1/2}}{\partial \delta} &= \frac{1}{2}K^{-1/2}\frac{\partial K}{\partial \delta} = -\frac{(\rho^{-2} - \frac{1}{2}J)}{\sqrt{K}} = -\sqrt{K} - \frac{J}{\sqrt{K}} = -Q_x - \frac{Q_y^2}{2Q_x} \\ \frac{\partial K_y^{1/2}}{\partial \delta} &= -\frac{1}{2}\sqrt{K} = -\frac{1}{2}Q_y\end{aligned}$$

   where we have assumed rectangular coordinates so that $\frac{\partial E_r}{\partial r} = \frac{\partial E_x}{\partial x} = -\frac{\partial E_y}{\partial y}$

2. The path length increases with energy, $\Delta P = 2\pi\eta\delta$. If the inner and outer quad plates have equal angular length, then a longer path corresponds to longer quads and more focusing.

$$\frac{\partial Q_{h/v}}{\partial \delta} = \sqrt{K_{x/y}}\eta = \frac{\eta}{R}Q_{h,v}$$

   where R is the magic radius. If the quad plates have equal linear length (rather than equal angular length), then there is no pathlength dependent focusing. The effect of pathlength will depend on the details of the fringe field at the ends of the quads.

3. The sextupole component of the quad fields couples to the tune via the dispersion. If the quad plates have no curvature, then the quadrupole symmetry precludes a sextupole moment. But there is curvature in the g-2 quads, and solutions to Laplace's equation in cylindrical coordinates are guaranteed a sextupole component. In cartesian coordinates the quadrupole potential

$$V(x,y) = \frac{1}{2}k(x^2 - y^2)$$

   gives

$$\mathbf{E} = -\nabla V = -kx\hat{\mathbf{x}} + ky\hat{\mathbf{y}}$$

   and $\frac{\partial E_x}{\partial x} + \frac{\partial E_y}{\partial y} = 0$. In cylindrical coordinates, a solution (but not a unique solution) to the Laplace equation with lowest order term linear in displacement, all of the nonlinearity in the radial coordinate, and a strictly linear vertical dependence is

$$V = k\left(\frac{1}{2}(r^2 - 1) - r_0 \ln\frac{r}{r_0} - y^2\right)$$

   and

$$\mathbf{E} = \frac{1}{2}k\left((r - \frac{r_0^2}{r})\hat{\mathbf{r}} - 2y\hat{\mathbf{y}}\right)$$

   With the substitution $r = r_0 + x$, where r_0 is the magic radius,

$$\begin{aligned}\mathbf{E} &= \frac{1}{2}k\left((r_0 + x - \frac{r_0^2}{r_0}[1 - \frac{x}{r_0} + \frac{1}{2}\left(\frac{x}{r_0}\right)^2 + \ldots])\hat{\mathbf{r}} - 2y\hat{\mathbf{y}}\right) \\ &\sim k\left(x - \frac{x^2}{2r_0} + \ldots)\hat{\mathbf{r}} - y\hat{\mathbf{y}}\right)\end{aligned}$$

The closed orbit for an off energy particle is shifted to $x \to \eta\delta + x$ and the radial component of the field for an off energy muon becomes

$$\begin{aligned} E_r &= k\left(x + \eta\delta - \frac{1}{2r_0}(x+\eta\delta)^2\right) \\ \frac{\partial E_r}{\partial x} &\to k(1 - \frac{1}{r_0}\eta\delta) \\ \frac{\partial\sqrt{K_x}}{\partial\delta} &= -\sqrt{K_x}\frac{\eta}{2r_0} \end{aligned}$$

The contribution to the chromaticity due to the quadratic component of the electric field is

$$\frac{\partial Q_h}{\partial\delta} = -\frac{\eta}{2r_0}\sqrt{K_x} = \frac{\eta}{2r_0}Q_x$$

In summary, contributions to chromaticity include

1. the energy dependence of the quad gradient and bend curvature
2. energy dependence of path length
3. nonlinearity associated with the curvature.

Assuming equal angular length of inner and outer plates and strictly linear vertical quad focusing (so that all of the nonlinearity due to curvature appears in the horizontal) the sum of the contributions is

$$\frac{\partial Q_x}{\partial\delta} = -Q_x - \frac{Q_y^2}{2Q_x} + Q_x\frac{\eta}{r_0} - Q_x\frac{\eta}{2r_0}$$

$$\frac{\partial Q_y}{\partial\delta} = -Q_y\left(\frac{1}{2} - \frac{\eta}{r_0}\right)$$

It turns out that for continuous focusing,

$$\eta = \frac{1}{Kr_0} = \frac{r_0}{Q_x^2}$$

Then

$$\frac{\partial Q_x}{\partial\delta} = -Q_x - \frac{Q_y^2}{2Q_x} + \frac{1}{Q_x}(1-\frac{1}{2}) = \frac{-1}{2Q_x} + \frac{1}{Q_x}(1-\frac{1}{2}) = 0$$

Evidently, if the inner and outer quad plates are equal angular length and if the quadratic correction to the quad field is restricted to the radial direction so the vertical is linear, then the horizontal chromaticity is identically zero. And the vertical can be written

$$\frac{\partial Q_v}{\partial\delta} = -Q_y\left(\frac{1}{2} - \frac{1}{Q_x^2}\right)$$

If, on the other hand, angular length is different for inner and outer plates, and/or Laplace's equation in cylindrical coordinates is satisfied by some nonlinearity in the vertical, rather than the horizontal, the chromatities will be very different. In order to get the chromaticity right, we need a 3D map of the quad fields that includes end effects as well as curvature.

Finally, suppose that all of the particles in the initial distribution appear in the ring at the same point in space and time but with a spread in energy. The particles will execute betatron oscillations with a frequency that depends on the energy, namely $Q_x(\delta) = Q'_x\delta$ and $Q_y(\delta) = Q'_y\delta$, where δ is the fractional energy offset. The particles will circulate with cyclotron frequencies $\frac{1}{\omega(\delta)} = \frac{1+\delta}{\omega_0}$. The betatron frequency

$$\begin{aligned} \omega_\beta &= Q\omega \quad \text{becomes} \\ \omega_\beta &\rightarrow (Q + Q'\Delta)\frac{\omega_0}{1+\Delta} \end{aligned}$$

6 Fast Rotation

Imagine that the initial distribution has zero emittance, zero energy spread and zero bunch length. The particles share a common revolution period T and the time dependence of the intensity signal at a fixed point in the ring (a fiber harp for example), is

$$I(t) = \delta(t - nT)$$

where n is any non negative integer. A particle with energy offset Δ will have revolution period $T(1 + \Delta)$, so that

$$I(t, \Delta) = \delta(t - nT(1 + \Delta))$$

The signal in the fiber harps is given by

$$S(t) = \sum_{n=0}^{\infty} \int \rho(\Delta)\delta(t - nT(1 + \Delta))d\Delta$$

where $\rho(\Delta)$ is the distribution of momenta offsets. If the energy distribution is Gaussian with width Δ_0, then

$$\begin{aligned} S(t) &= \sum_{n=0}^{\infty} \int \frac{e^{-\Delta^2/(2\Delta_0^2)}}{\sqrt{2\pi}\Delta_0}\delta(t - nT(1 + \Delta))d\Delta \\ &= \sum_{n=0}^{\infty} \int \frac{e^{-\Delta^2/(2\Delta_0^2)}}{\sqrt{2\pi}\Delta_0}\frac{\delta(\Delta - (\frac{t}{nT} - 1)}{nT}d\Delta \\ &= \sum_{n=0}^{\infty} \frac{e^{-(\frac{t}{nT}-1)^2/(2\Delta_0^2)}}{\sqrt{2\pi}\Delta_0 nT} \end{aligned} \tag{6}$$

For energy spread $\Delta_0 = 0.0012$, which is just about the acceptance of the g-2 ring, $S(t)$ from Equation 6 is shown in Figures 8, 9, and 10. Figures 9, and 10 are the same data as 8 on expanded horizontal scale. The intensity asymptotically approaches that of the average stored current $\langle I \rangle = eN_\mu/T$. (Note that there is no muon decay in Equation 6 or the accompanying plots).

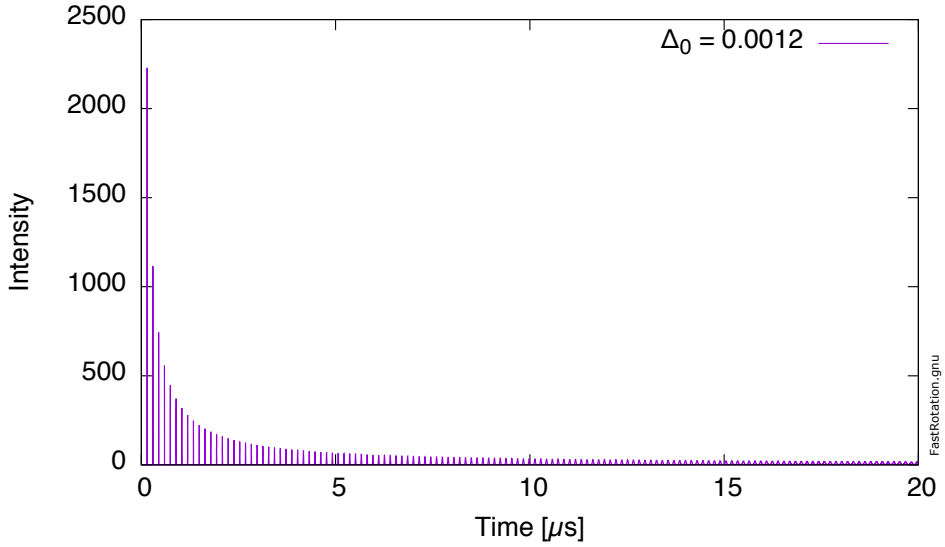

Figure 8: Fast rotation signal 0-20μs. (See script for plotting with *gnuplot* in Appendix.)

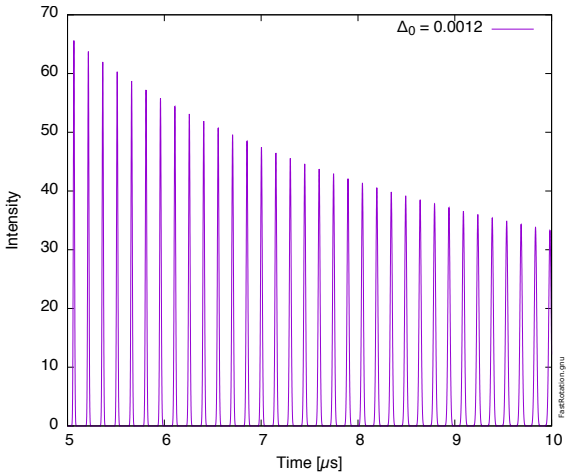

Figure 9: Fast rotation signale from 5μs to 10μs

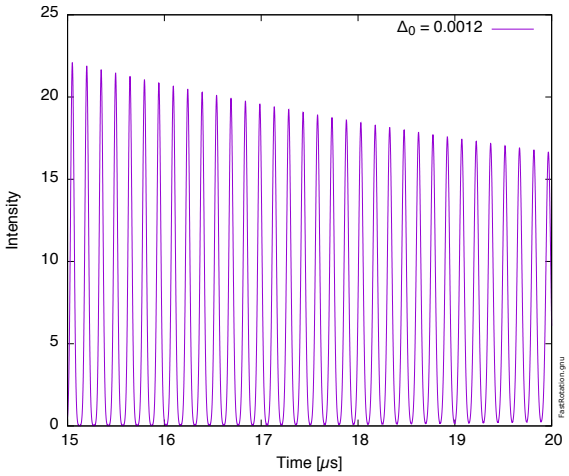

Figure 10: Fast rotation signal from 15μs to 20μs.

6.1 Momentum distribution from fast rotation signal

An established method for extracting the energy (or equivalently frequency) distribution is to take the real part of the fourier transform of the fast rotation signal[2]. Let's try that out.

$$\begin{aligned}
F(\omega,t_0) &= \int_0^\infty S(t,\Delta_0)\cos\omega(t-t_0)dt \\
&= \sum_{n=0}^{\infty}\int_0^\infty \frac{e^{-(\frac{t}{nT}-1)^2/(2\Delta_0^2)}}{\sqrt{2\pi}\Delta_0 nT}\cos\omega(t-t_0)dt \\
&= \sum_{n=0}^{\infty}\int_0^\infty \frac{e^{-t^2/(2(nT)^2\Delta_0^2)+t/(nT\Delta_0^2)\pm i\omega t}e^{\mp i\omega t_0}e^{-1/(2\Delta_0^2)}}{\sqrt{2\pi}\Delta_0 nT} \\
&= \frac{1}{2}\sum_{n=0}^{\infty} e^{(1/(nT\Delta_0^2)\pm i\omega t)^2)((nT)^2\Delta_0^2)/2}e^{\mp i\omega t_0}e^{-1/(2\Delta_0^2)} \\
&= \sum_{n=0}^{\infty} e^{(1/(nT\Delta_0^2)^2-(\omega t)^2))((nT)^2\Delta_0^2)/2}e^{-1/(2\Delta_0^2)}\cos\omega(nT-t_0) \\
&= \sum_{n=0}^{\infty} e^{(1/(2\Delta_0^2)-\omega^2(nT)^2\Delta_0^2/2)}e^{-1/(2\Delta_0^2)}\cos\omega(nT-t_0) \\
F(\omega,t_0) &= \sum_{n=0}^{\infty} e^{-\omega^2(nT)^2\Delta_0^2/2}\cos\omega(nT-t_0) \qquad (7)
\end{aligned}$$

The fourier transform of the fast rotation signal for a distribution with $\Delta E/E = 0.0012$, zero emittance and zero bunch length is shown in Figures 11– 12. The rotation harmonics out to 200 MHz are shown in Figure 11. The part of the frequency distribution in the band corresponding to particles inside the vacuum chamber is Figure 12 along with a Gaussian of width $\Delta f/f = 0.0012$. Sure enough the Fourier transform of the fast rotation signal reproduces the energy spread of the distribution.

7 Bunch Length

Next introduce finite bunch length. Referring back to Equation 6 it is straightforward to include a temporal offset t' into the fast rotation signal as follows

$$S(t,t') = \sum_{n=0}^{\infty}\frac{e^{-(\frac{t-t'}{nT}-1)^2/(2\Delta_0^2)}}{\sqrt{2\pi}\Delta_0 nT}$$

Suppose the intial temporal (longitudinal) distribution of the muons is Gaussian

$$\xi(t') = \frac{1}{\sqrt{2\pi}\sigma_t}e^{-t'^2/(2\sigma_t^2)}$$

Then

$$S(t) = \sum_{n=0}^{\infty}\int_{-\infty}^{\infty} dt'\frac{e^{-(\frac{t-t'}{nT}-1)^2/(2\Delta_0^2)}}{\sqrt{2\pi}\Delta_0 nT}\frac{1}{\sqrt{2\pi}\sigma_t}e^{-t'^2/(2\sigma_t^2)}$$

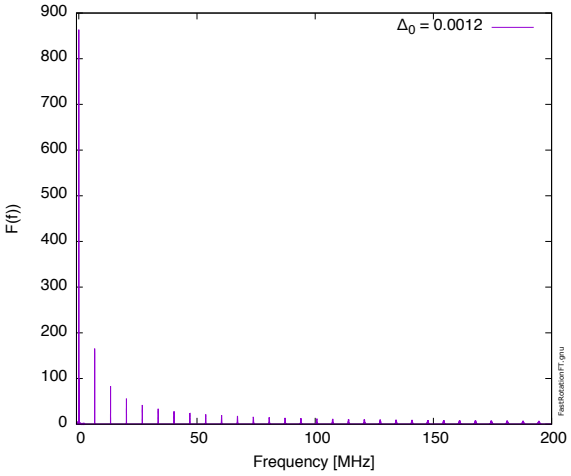

Figure 11: Real part of fourier transform of fast rotation signal shown in Figure 8.

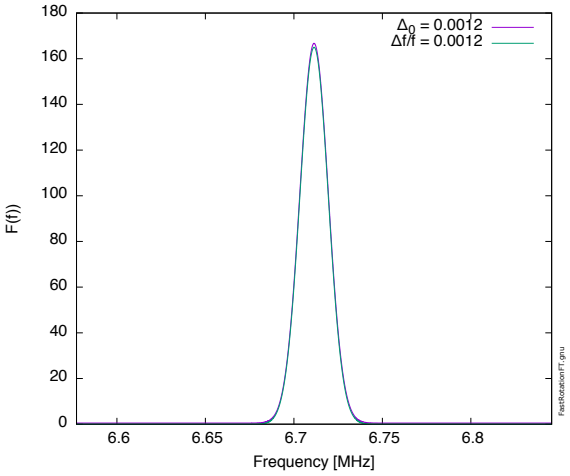

Figure 12: Real part of fourier transform of fast rotation signal in Figure 8 within the acceptance of the vacuum chamber. A Gaussian with $\sigma_f/f = 0.0012$ is superimposed.

$$
\begin{aligned}
&= \sum_{n=0}^{\infty} \frac{1}{2\pi\Delta_0 nT\sigma_t} \int_{-\infty}^{\infty} dt' e^{-(\frac{t-t'}{nT}-1)^2/(2\Delta_0^2)} e^{-t'^2/(2\sigma_t^2)} \\
&= \sum_{n=0}^{\infty} \frac{1}{2\pi\Delta_0 nT\sigma_t} e^{-t^2/(2(nT\Delta_0)^2)} \int_{-\infty}^{\infty} dt' e^{-(\frac{t'^2-2tt'}{(nT)^2}+1-\frac{2(t-t')}{nT})/(2\Delta_0^2)} e^{-t'^2/(2\sigma_t^2)} \\
&= \sum_{n=0}^{\infty} \frac{1}{2\pi\Delta_0 nT\sigma_t} e^{-t^2/(2(nT\Delta_0)^2)} e^{\frac{t}{nT\Delta_0^2}} \int_{-\infty}^{\infty} dt' \exp(-t'^2(\frac{1}{2(nT)^2\Delta_0^2}+\frac{1}{2\sigma_t^2}) + t'(\frac{t}{nT}-1)/(nT\Delta_0^2)) e^{-1/(2\Delta_0^2)} \\
&= \sum_{n=0}^{\infty} \frac{1}{2\pi\Delta_0 nT\sigma_t} e^{-(\frac{t}{nT}-1)^2/2\Delta_0^2} \int_{-\infty}^{\infty} dt' \exp\left(-\alpha t'^2 + \beta t'\right) \\
&= \sum_{n=0}^{\infty} \frac{1}{2\pi\Delta_0 nT\sigma_t} e^{-(\frac{t}{nT}-1)^2/(2\Delta_0^2)} \sqrt{\frac{\pi}{\alpha}} e^{\beta^2/4\alpha}
\end{aligned}
$$

where $\alpha = \frac{1}{2(nT)^2\Delta_0^2} + \frac{1}{2\sigma_t^2}$ and $\beta = (\frac{t}{nT}-1)/(nT\Delta_0^2)$. Finally

$$
\begin{aligned}
S(t) &= \sum_{n=0}^{\infty} \frac{1}{2\pi\Delta_0 nT\sigma_t} e^{-(\frac{t}{nT}-1)^2/(2\Delta_0^2)} \frac{\sqrt{2\pi} nT\Delta_0\sigma_t}{\sqrt{(nT)^2\Delta_0^2+\sigma_t^2}} \exp(\frac{(\frac{t}{nT}-1)^2}{(nT\Delta_0^2)^2} \frac{(nT)^2\Delta_0^2\sigma_t^2}{2(nT)^2\Delta_0^2+2\sigma_t^2}) \\
&= \frac{1}{\sqrt{2\pi}} \sum_{n=0}^{\infty} e^{-(\frac{t}{nT}-1)^2/(2\Delta_0^2)} \frac{1}{\sqrt{((nT)^2\Delta_0^2+\sigma_t^2}} \exp(\frac{(\frac{t}{nT}-1)^2}{\Delta_0^2} \frac{\sigma_t^2}{2(nT)^2\Delta_0^2+2\sigma_t^2}) \\
&= \frac{1}{\sqrt{2\pi}} \sum_{n=0}^{\infty} \frac{1}{\sqrt{((nT)^2\Delta_0^2+\sigma_t^2}} \exp(\frac{-(\frac{t}{nT}-1)^2}{2\Delta_0^2} \left(1 - \frac{\sigma_t^2}{(nT)^2\Delta_0^2+\sigma_t^2}\right)) \qquad (8)
\end{aligned}
$$

Let's look at a couple of examples. Figure 13 shows the first 20 μs of the fast rotation signal of a distribution with Gaussian energy spread $\Delta E/E = 0.0012$ and pulse length σ_t =20ns. This is to be compared with Fig. 8 with $\sigma_t = 0$. Figure 14 is the fast rotation signal for a distribution with the same energy spread but pulse length $\sigma_t = 60$ns, closer to what we will see in E989.

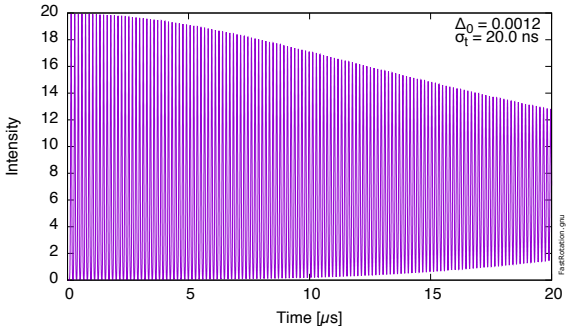

Figure 13: Fast rotation signal from a muon pulse with Gaussian energy spread $\Delta E/E = 0.0012$ and Gaussian temporal spread $\sigma_t = 20$ns.

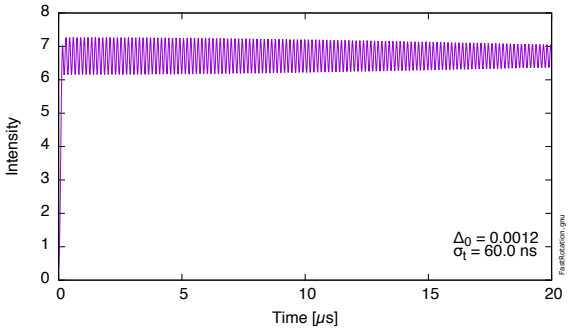

Figure 14: Fast rotation signal from muon pulse with $\Delta E/E = 0.0012$, and $\sigma_t = 60$ns.

It will turn out to be convenient to rewrite Equation 8 as

$$S(t) = \frac{1}{\sqrt{2\pi}} \sum_{n=0}^{\infty} \frac{1}{\sqrt{((nT)^2 {\Delta_0'}^2}} \exp\left(\frac{-(\frac{t}{nT} - 1)^2}{2{\Delta_0'}^2}\right) \quad (9)$$

where

$${\Delta_0'}^2 = \frac{(nT\Delta_0)^2 + \sigma_t^2}{(nT)^2}$$

Then it is easy to see that the Fourier transform has the same form as Equation 7 and

$$F(\omega, t_0, \Delta_0') = \sum_{n=0}^{\infty} e^{-\omega^2 (nT)^2 {\Delta_0'}^2/2} \cos\omega(nT - t_0) \quad (10)$$

Examples of fourier transforms (Equation 9) of the fast rotation signal for distributions with energy width $\Delta E/E = 0.0012$ and lengths $\sigma_t = 20$ns and $\sigma_t = 60$ ns respectively are shown in Figure 15 over the frequency range consistent with the chamber aperture. For both cases the distribution is Gaussian with width $\Delta f/f = 0.0012$ so that the Fourier transform does indeed reproduce the energy spread independent of pulse length. The effect of the bunch length is to reduce the amplitude of the signal. At what point the signal is dominated by statistical noise remains to be determined.

8 Energy and dispersion

The final focus of the M5 line is designed with zero dispersion at the exit of the inflector[3] so muons entering the ring with fractional energy offset Δ, will oscillate transversely about the corresponding

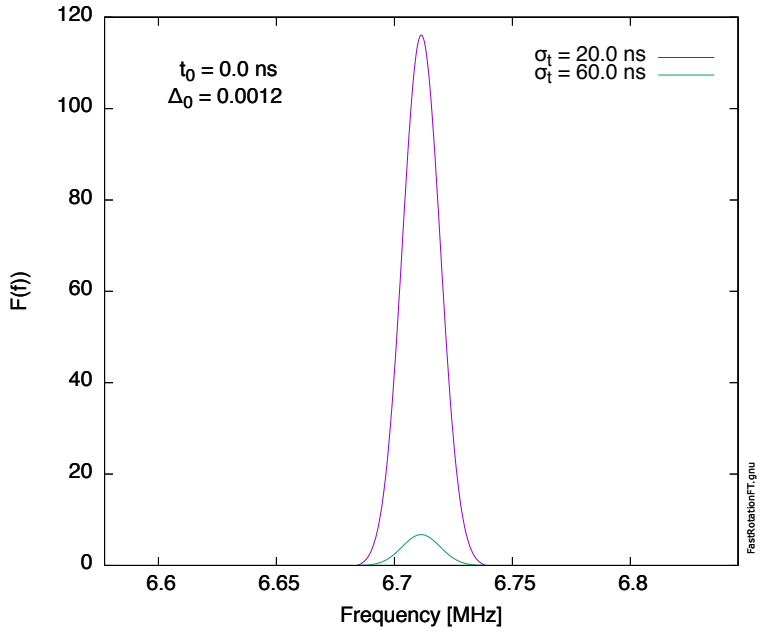

Figure 15: Fourier transform of fast rotation signal for distributions with pulse length $\sigma_t = 20$ns and $\sigma_t = 60$ns. (See script for plotting with *gnuplot* in Appendix.)

closed orbit ($x_c(\Delta) = \eta\Delta$) with amplitude $x(\Delta) = \eta\Delta$ and frequency

$$f = Q\omega_0 \rightarrow (Q + Q'\Delta)\frac{\omega_0}{1+\Delta}$$

where ω_0 is the revolution frequency of the magic momentum muon, and Q and Q' are the horizontal betatron tune and chromaticity, (discussed above) respectively. The time dependent transverse motion of a single muon with energy offset Δ is

$$x(t) = \eta\Delta(1 - \cos\left((Q + Q'\Delta)\frac{\omega_0 t}{1+\Delta}\right)$$

Then the position at a fixed point in the ring s, is

$$x(t,\Delta)_s = \sum_n \eta\Delta\left(1 - \cos\left((Q + Q'\Delta)\frac{\omega_0}{1+\Delta}t\right)\right)\delta(t - nT(1+\Delta))$$

$$x(t,\Delta)_s = \sum_n \eta\Delta\left(1 - \cos\left((Q + Q'\Delta)\frac{\omega_0}{1+\Delta}t\right)\right)\delta(\Delta - (\frac{t}{nT} - 1))$$

Next consider a distribution with zero emittance and zero length, but finite Gaussian energy spread,

$$\rho(\Delta) = \frac{e^{-\frac{\Delta^2}{\Delta_0^2}}}{\sqrt{2\pi}\Delta_0}$$

Averaging over all energy offsets we find

$$\begin{aligned} N\langle x(t)\rangle &= \int_{-\infty}^{\infty} d\Delta \sum_n \eta\Delta(\left(1-\cos\left((Q+Q'\Delta)\frac{\omega_0}{1+\Delta}t\right)\right)\frac{e^{-\frac{\Delta^2}{2\Delta_0^2}}}{\sqrt{2\pi}\Delta_0}\delta(\Delta-(\frac{t}{nT}-1)) \\ &= \sum_n \eta(\frac{t}{nT}-1)\left(1-\cos\left((Q+Q'(\frac{t}{nT}-1))\frac{\omega_0}{t/nT}t\right)\right)\frac{e^{-\frac{(\frac{t}{nT}-1)^2}{2\Delta_0^2}}}{\sqrt{2\pi}\Delta_0} \\ &= \sum_n \eta(\frac{t}{nT}-1)\left(1-\cos\left((QnT+Q'(t-nT))\omega_0\right)\right)\frac{1}{\sqrt{2\pi}\Delta_0}e^{-\frac{(\frac{t}{nT}-1)^2}{2\Delta_0^2}} \end{aligned}$$

$N\langle x(t)\rangle$ is the average position at time t, weighted by the number of muons at that time. In order to extract the average position independent of number, divide by

$$N = \sum_n \frac{1}{\sqrt{2\pi}\Delta_0}e^{-\frac{(\frac{t}{nT}-1)}{2\Delta_0^2}}$$

so that

$$\langle x(t)\rangle = \frac{1}{N}\sum_n \eta(\frac{t}{nT}-1)\left(1-\cos\left((QnT+Q'(t-nT))\omega_0\right)\right)\frac{1}{\sqrt{2\pi}\Delta_0}e^{-\frac{(\frac{t}{nT}-1)^2}{2\Delta_0^2}} \tag{11}$$

The average centroid displacement at a fixed point in the ring (for example at a fiber harp) is given by Equation 11 and plotted in Figure 16 at 1ns intervals, for an initial distribution with Gaussian energy width $\Delta_0 = 0.0012$, zero pulse length and zero emittance. The betatron motion begins to evolve in the first few turns after injection and then decoheres on a time scale of 30μs. The frequency of the envelope of the turn by turn motion, most apparent in the first 20μs (Fig. 17) is the betatron tune ($f_\beta = Q\omega_0$). A coherent oscillation of the centroid persists beyond 100μs (Fig. 18.)

We attempt to reproduce the analytic result in a "realistic" tracking simulation. Figures 19– 22 are simulation data with the BMAD model of the storage ring, including collimators and quadrupole nonlinearity (which are of course not part of the analytic calcuation). The distribution has Gaussian energy width $\Delta E/E = \Delta_0$, pulse length $\sigma_t = 1$ns (that is, approximately zero) and zero emittance. The muon distribution is injected on axis, mimicing a perfect kick. Nevertheless, a coherent betatron oscillation emerges as the envelope of the fast rotation signal. Immediatelay after injection, there is zero coherent oscillation. As long as the average momentum is the magic momentum, the average displacement is zero. The betatron oscillations of the high and low momentum muons are 180 deg out of phase. Coherent oscillations appear as the high momentum muons lag behind the low momentum particles. Also, because the momentum spread of the distribution at the inflector exit is greater than the momentum acceptance of the ring, the amplitude of the coherent oscillations arising from the momentum spread will by definition fill the aperture.

One thing to keep in mind: the time dependence of the centroid motion at a fixed point in the ring as shown in Figures 19– 22, etc. will depend on the width of the time bin, which here is 1ns. As the width of the time bin increases the average displacement of the distribution decreases, approaching zero as the time bin approaches the revolution period of 149 ns. Note also that each point in the Figures will in general correpond to the average of the positions of only those muons in

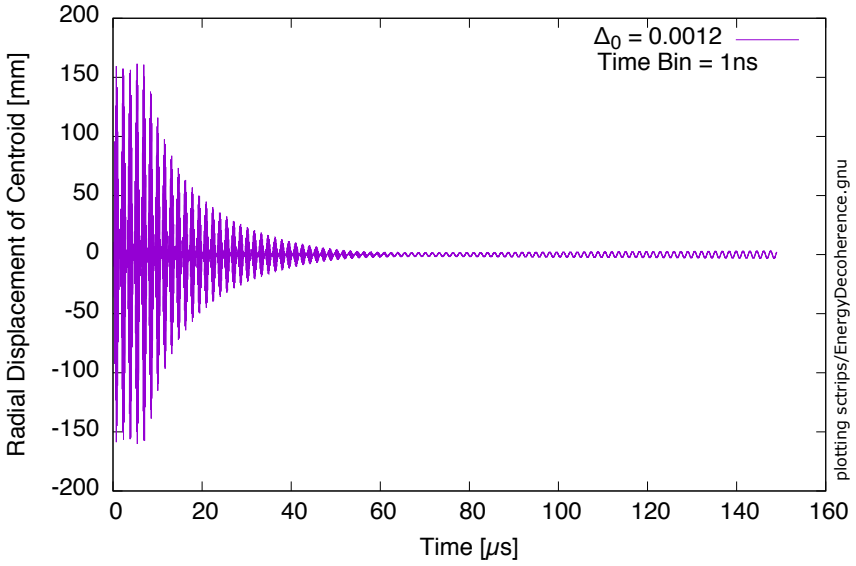

Figure 16: Centroid motion of a distribution with Gaussian energy width, $\Delta E/E = 0.0012$, zero length and zero emittance, from Equation 11 evaluated at 1ns intervals.

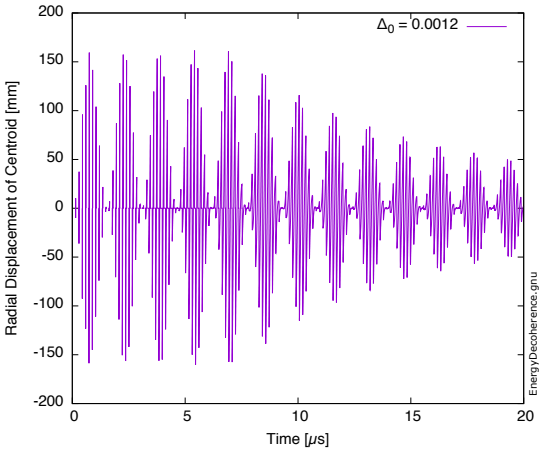

Figure 17: Centroid motion (Equation 11) for the same distribution as Fig. 16 for the first 20μs after injection. The frequency of the envelope is the betatron tune.

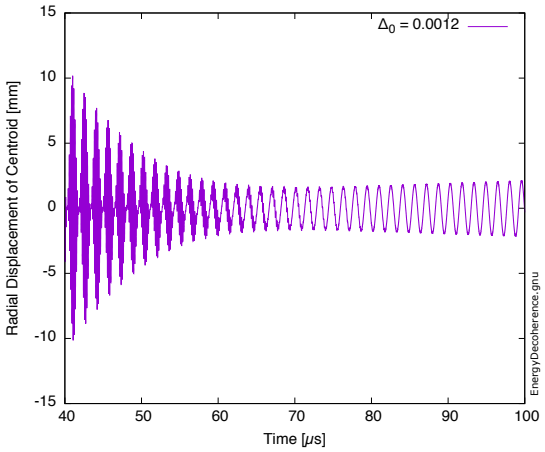

Figure 18: Centroid motion (Equation 11) for the same distribution as Fig. 16, 40-100μs after injection.

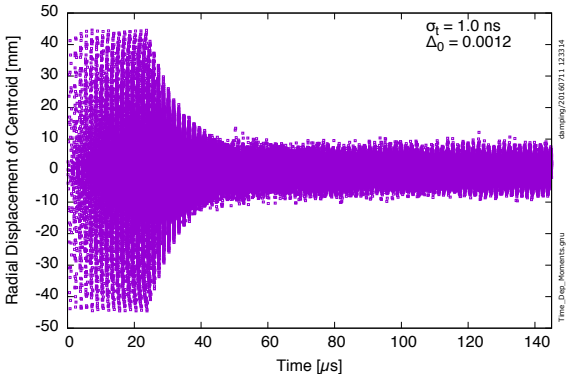

Figure 19: Simulated centroid motion for a distribution with Gaussian energy width $\Delta E/E = 0.0012$, zero length, and zero emittance. The distribution is injected on axis into the ring, so that there is initially no coherent betatron oscillation. Centroid motion evolves with time due to the momentum spread.

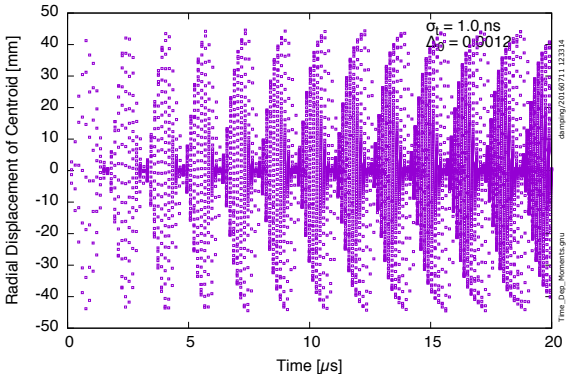

Figure 20: Simulated centroid motion for the same distribution as Fig. 19 for the first 20μs after injection. The coherent oscillation of the centroid is evident. The centroid motion is modulated at the betatron tune.

that particular time bin. As a result, some points will represent the average of a very few muons. It is after all, a plot of average position versus time, with no accounting for intensity. It is clear again in Fig. 22 that a coherent oscillation persists well beyond 100 μs, albeit with relatively small amplitude of $\pm$5mm.

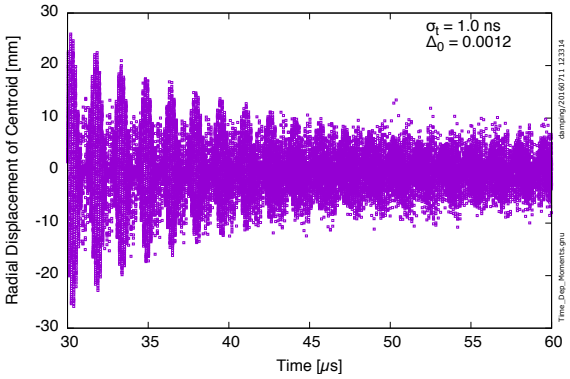

Figure 21: Simulated centroid motion for the same distribution as Fig. 19 from 30-60μs after injection. The decoherence time is about 30μs.

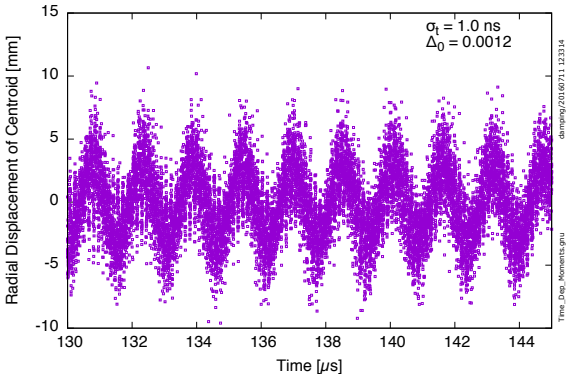

Figure 22: Simulated centroid motion for the same distribution as Fig. 19 130-145μs after injection. Some coherent motion persists well beyond 100μs.

9 Put the pieces together

Finally consider a more realistic distribution with finite energy spread, 95% of beam particles within 40mm-mrad emittance, and temporal distribution anticipated for E989[4] as shown in the Appendix in Figure 34.The simulated centroid motion that would be measured at a thin detector at a fixed point in the ring, with 1ns time bin width is shown in Figures 25– 26. The coherent centroid motion that arises due to the dispersion mismatch and momentum spread is evident, although here (as compared to Figures 19– 22) mitigated by the larger emittance and the longer pulse duration. Some coherent motion persists for more than 1000 turns (149μs). Remember that the distribution is initialized on the magic radius, as if it were injected with the perfect kick.

Let's try one more thing. Suppose the kicker pulse is imperfect and there is some displacement or angle of the injected muons with respect to the closed orbit and a coherent oscillation of the centroid. The time dependence of the centroid is shown in Figures 27 - 28 for a distribution with emittance 40 mm-mrad, energy spread $\Delta E/E = 0.0012$, 'W' shaped pulse, and kick angle error of 2 mrad (out of 10.6 mrad). To see the effect of the kick error, compare Figure 27 to Figure 24. For times longer than 100μs the coherent centroid oscillation is very nearly independent of the kick error. (Figure 28 versus Figure 26).

The time dependence of the width of the distribution is shown in Figures 29– 30.

10 Summary

The irreducible momentum spread in the muon distribution emerges as a coherent oscillation of the distribution centroid. This continues to be the case for the anticipated "W" temporal shape, and realistic transverse emittance. The CBO associated with the momentum spread persists at some level beyond 145μs. Coherent centroid motion at $t = 0$ results from a kicker error. This component of the CBO decoheres on the time scale of 100μs due to quadrupole nonlinearity.

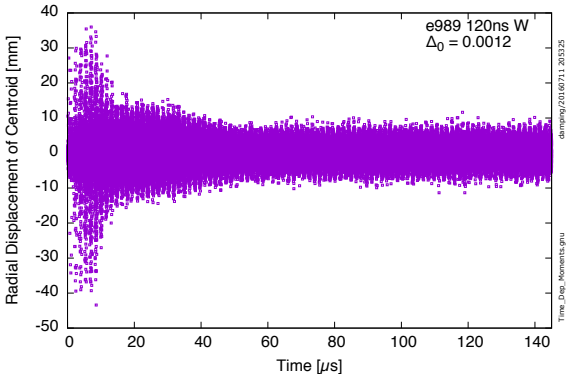

Figure 23: Simulation of centroid motion of distribution with finite emittance (40 mm-mrad) and 'W' pulse shape, and energy spread = 0.0012

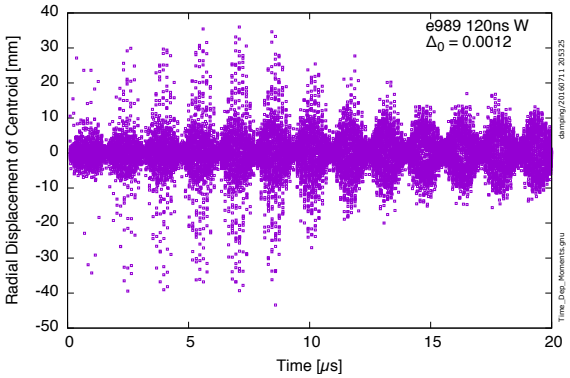

Figure 24: Simulation of centroid motion for distribution with finite emittance and 'W' pulse shape, and energy spread =0.0012

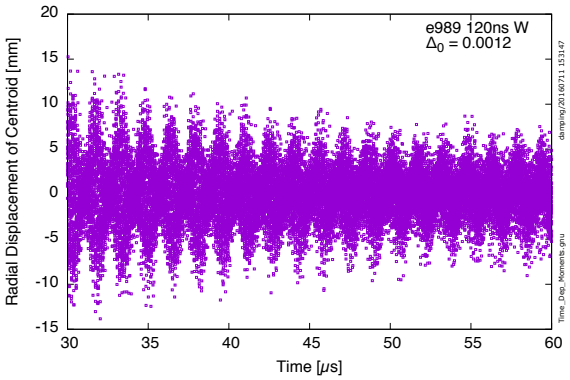

Figure 25: Simulation of centroid motion for distribution with finite emittance, 'W' pulse shape, energy spread = 0.0012

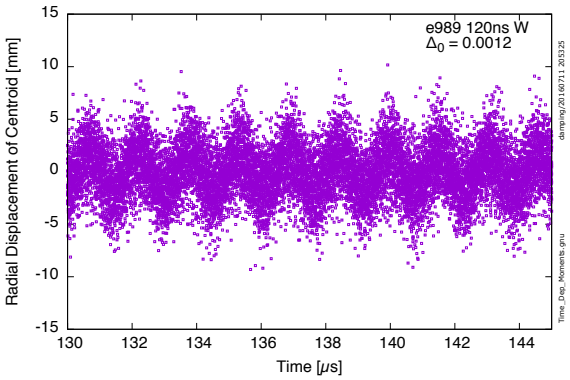

Figure 26: Simulation of centroid motion for distribution with finite emittance, 'W' pulse shape, and energy spread=0.0012

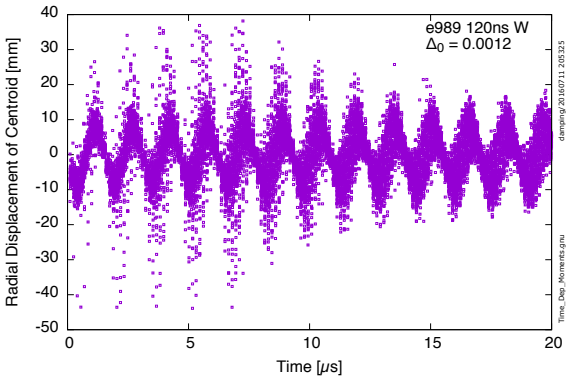

Figure 27: Finite emittance and W pulse shape, energy spread = 0.0012, kick error = 2mrad

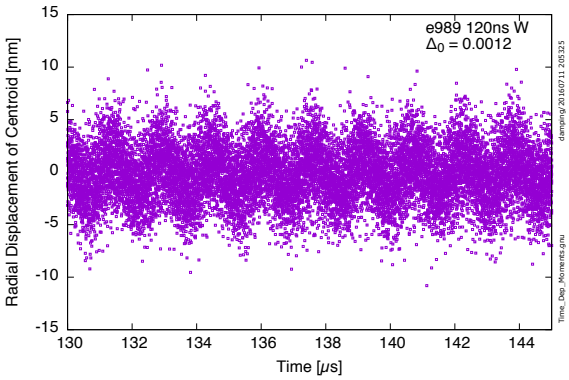

Figure 28: Finite emittance and W pulse shape, energy spread, kick error = 2mrad

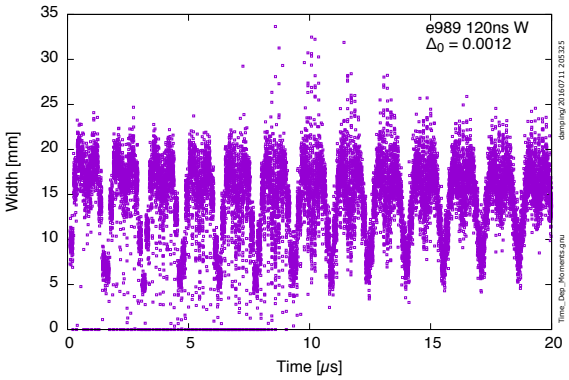

Figure 29: Finite emittance and W pulse shape, energy spread = 0.0012, kick error

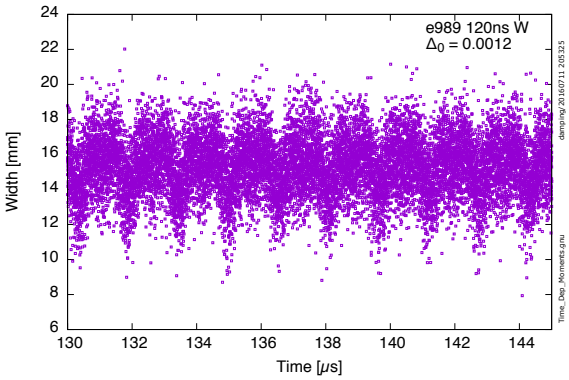

Figure 30: Finite emittance and W pulse shape, energy spread, kick error

11 Appendix

11.1 Fourier transform of fast rotation signal

As shown above, the real part of the Fourier transform of the fast rotation signal of a Gaussian distribution of energies with $\sigma_E/E = 0.0012$ is given by

$$F(\omega, \Delta_0, t_0) = \sum_{n=0}^{\infty} e^{-\omega^2 (nT)^2 \Delta_0^2/2} \cos\omega(nT - t_0) \tag{12}$$

At the moment that the muons enter the ring, there is presumably no correlation between muon momentum and time. The measurement of the fast rotation signal necessarily begins at some time $t_s > t_0$ after some energy-time correlation has already evolved. We measure $S(t)$ but we are forced to estimate t_0. The symmetry of the fourier transform $F(\omega, \Delta_0, t_0)$ is sensitive to the error in t_0. According to the algorithm described by Orlov et.al.[2], we can refine our estimate of t_0 by finding the value that best symmetrizes $F(\omega)$. $F(\omega, \Delta_0, t_0)$ for a various values of the start time offset t_0 are shown in Figures 31 - 33, demonstrating the dependence of the symmetry of the transform to t_0.

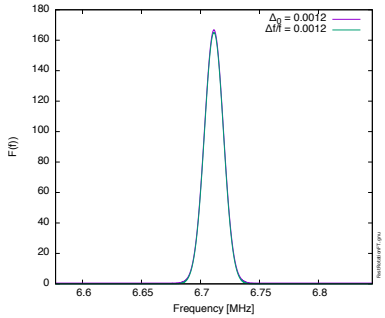

Figure 31: Real part of fourier transform of fast rotation signal shown in Figure 8. Gaussian with width $\Delta f/f = 0.0012$ is superimposed. $t_0 = 0$.

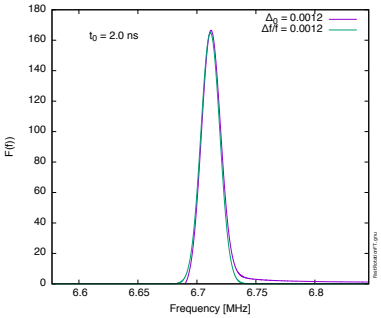

Figure 32: Same as Figure 32 but with $t_0 = 2$ns (see Equation 12).

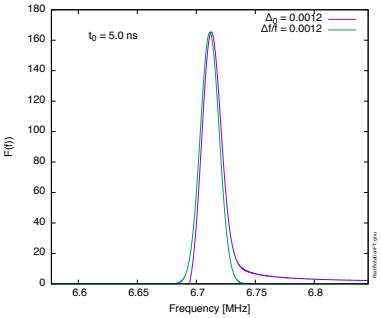

Figure 33: Same as Figure 33 but with $t_0 = 5$ns.

11.2 Gnuplot plotting scripts

The script for plotting the analytic form of the fast rotation signal and its fourier transform are included for reference.

gnuplot script for plotting Fast Rotation Signal (Equation 8)

```
set terminal pdf enhanced fontscale 0.75 size 6.0in, 3.5in
set output 'FastRotation.pdf'
f(x,n) = exp(-(x/n/Trev -1)**2/2/d0**2)/sqrt(2*pi)/d0/n/Trev
g(x,n) = exp(-(x/n/Trev -1)**2/2/d0**2*(1-sigt**2/((n*Trev*d0)**2+sigt**2)))/sqrt(2*pi)/sqrt((n*d0*Trev)**2 + sigt**2)
```

```
Trev=149.e-9*1.e6
sigt=20.e-9*1.e6
d0=0.0012
set xrange [0:20]
set samples 5000  #increase sample size to show more detail
set ylabel 'Intensity'
set xlabel 'Time [{/Symbol m}s]'
unset label
set label 'FastRotation.gnu' at graph 1.02,0.02 rotate left font 'Verdana,6'
delta0 = sprintf("%.4f",d0)
sigmat = sprintf("%3.1f",sigt*1.e3)
set label  '{/Symbol D}_0 = '.delta0 at graph 0.8,0.95
set label '{/Symbol s}_t = '.sigmat.' ns' at graph 0.8,0.9
plot '+' using 1:(sum [n=1:1000] g($1,n)) w l not
```

gnuplot script for plotting Fourier Transform of Fast Rotation Signal (Equation 10) as in Figure 15

```
set terminal pdf enhanced fontscale 0.75 size 6.0in, 5.0in
set output 'FastRotationFT.pdf'
f(x,n) = exp(-(2*pi*x*n*Trev)**2*((n*Trev*d0)**2+sigt**2)/(n*Trev)**2/2)*cos(2*pi*x*(n*Trev-t0))
Trev=149.e-3
freq=1./Trev
omega=2*pi*freq
d0=0.0012
t0=0.0
sigt=20.e-3
set xrange [0.98*freq:freq*1.02]
#set xrange [-1:200]
unset label
set yrange [0:]
set samples 1000
set ylabel 'F(f))'
set xlabel 'Frequency [MHz]'
set key spacing 1.5 height 1
set label 'FastRotationFT.gnu' at graph 1.02,0.02 rotate left font 'Verdana,6'
delta0 = sprintf("%.4f",d0)
df=0.008
df0 = sprintf("%.4f",df/freq)
t0w = sprintf("%.1f",t0*1e3)
sigtw = sprintf("%.1f",sigt*1e3)
A=165
set label at graph 0.1,0.9 '  t_0 = '.t0w.' ns'
#set label at graph 0.1,0.85 '  {/Symbol s}_t = '.sigtw.' ns'
set label at graph 0.1,0.85 '{/Symbol D}_0 = '.delta0
stats '+' using 1:(sum [n=1:1000] f($1,n))
```

```
ff(x) = STATS_max_y*exp(-(x-freq)**2/2./df**2)
set multiplot
set yrange [0:120]
plot '+' using 1:(sum [n=1:1000] f($1,n)) w l lc 1 t '{/Symbol s}_t = '.sigtw.' ns'
sigt=60.e-3
sigtw = sprintf("%.1f",sigt*1e3)
set key height 2.1
plot  '+' using 1:(sum [n=1:1000] f($1,n)) w l lc 2 t '{/Symbol s}_t = '.sigtw.' ns'
unset multiplot
```

11.3 Pulse shape

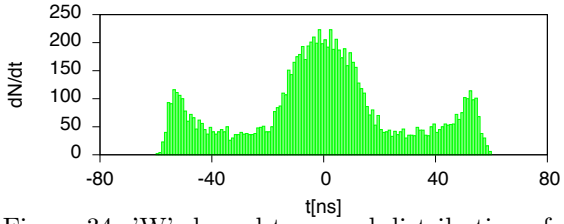

Figure 34: 'W'-shaped temporal distribution of the muon pulse

References

[1] Yannis K. Semertzidis, Gerald Bennett, Efstratios Efstathiadis, Frank Krienen, Richard Larsen, Y.Y. Lee, William M. Morse, Yuri Orlov, Cenap S. Ozben, B. Lee Roberts, Louis P. Snydstrup, David S. Warburton. *The Brookhaven muon (g-2) storage ring high voltage quadrupole.* Nuclear Instruments and Methods in Physics Research A 503 (2003) 458484

[2] Yuri Orlov, Cenap S. Ozben, and Yannis K. Semertzidis. *Muon revolution frequency distribution from a partial-time Fourier transform of the g-2 signal in the muon g-2 experiment.* Nuclear Instruments and Methods in Physics Research A 482 (2002) 767775

[3] D. Rubin. *Beam Dynamics Injection and Storage.* G-2 Experiment Document 2820-v5

[4] GM2-doc-1931-v1, Chapter 7, page 135